



Coastal surface soil carbon stocks have distinctly increased under extensive ecological restoration in northern China

Yuan Chi ^{1✉}, Dahai Liu ^{1✉}, Jianhua Gao^{2✉}, Jingkuan Sun³, Zhiwei Zhang^{1,2}, Wenxiu Xing¹, Yubing Qu^{1,2}, Xuejian Ma¹ & Bian Zha²

Coastal soil carbon stock is critical owing to the coexistence of terrestrial and marine carbon sinks and undergoes drastic changes under complex factors. Here we conduct surface soil organic carbon (SOC) stock mapping in northern China's coastal areas in 2020 and 2010 based on large-scale field survey, remote sensing, and land cover data. Our results indicate that a 100 m resolution is the optimum mapping resolution for its good simulation accuracy and precise spatial details. The surface SOC stock and density in 2020 increased by 39.19% and 37.82%, respectively, compared with those in 2010 under extensive ecological restoration. The SOC densities of forests, grasslands, croplands, wetlands, and built-up areas increased by 72.58%, 74.25%, 41.39%, 4.58%, and 26.30% from 2010 to 2020, respectively. The study determines the optimum mapping resolution and denotes the positive effects of ecological restoration on coastal soil carbon.

¹Key Laboratory of Coastal Science and Integrated Management, First Institute of Oceanography, Ministry of Natural Resources, Qingdao 266061, China. ²School of Geography and Ocean Science, Nanjing University, Nanjing 210023, China. ³Shandong Key Laboratory of Eco-Environmental Science for the Yellow River Delta, Binzhou University, Binzhou 256603, China. ✉email: chiyuan@fio.org.cn; liudahai@fio.org.cn; jhgao@nju.edu.cn

Soil is one of the largest carbon pools on Earth and plays a vital role in global biogeochemical cycles under the background of climate change^{1,2}. The coastal soil carbon stock is enormous owing to the blue carbon sequestered by wetland vegetation^{3,4} and the green carbon sequestered by coastal upland forests⁵, while demonstrates remarkable spatiotemporal variations due to intensive land-sea interaction⁶ and increasing human activities⁷ in recent decades. Shifts in the coastline caused by natural deposition-erosion processes^{8,9} and anthropogenic coastal engineering¹⁰, along with changes in land surface characteristics controlled by human activities^{11,12}, shape the spatial pattern of coastal soil carbon stock. In addition, during the last decade in China, extensive ecological restoration projects have been implemented at the national scale^{13,14}, dominating vegetation greening¹⁵, improving habitat quality¹⁶, and thus influencing the large-scale pattern of soil carbon stock¹⁷, particularly in the surface soil, which is the most sensitive soil layer to land surface characteristics¹⁸. It is of great significance to map the spatiotemporal pattern of coastal soil carbon stock at a large scale during the last decade to effectively grasp the overall and spatial characteristics of coastal blue and green carbon in the context of extensive ecological restoration.

The core issue in large-scale coastal soil carbon stock mapping is accuracy, which creates a high demand on four points. The first is field soil data, which serve as the basis of soil mapping; however, they are costly at a large scale¹⁹ and are always discontinuous across different time points¹⁸, thereby limiting the large-scale soil carbon mapping across time points. The second is the predictors, which are used as the covariates of field point data and to realize the from point to area conversion of the soil data^{20,21}. Predictors are essential for soil carbon mapping; however, their comprehensiveness and applicability are always incompatible because of the data availability problem²². The third is the spatial resolution, which refers to the minimum simulation unit in the mapping and indicates the spatial details of the results^{23,24}. Coarse resolution (≥ 1000 m) was always adopted in studies on large-scale soil carbon mapping^{25–27}, while fine resolution can be observed in several studies, which, however, remained in a static state at a single time point^{28–30}. The fourth is the simulation accuracy, which finally denotes the mapping effect^{31,32} and is determined by multiple factors, including the number and distribution of field soil data^{33,34}, the comprehensiveness and applicability of predictors^{35,36}, and the fitness of simulation unit^{37,38}. The four aforementioned points can be summarized as follows: Sufficient field soil data should be collected, suitable predictors that cover the study area should be selected, and optimum spatial resolution should be adopted to achieve high simulation accuracy and precise spatial details in large-scale coastal soil carbon stock mapping.

In the present study, large-scale coastal soil carbon stock mapping was conducted to correspond to the aforementioned four key points using the northern China's coastal areas as the scope, which range from 31°N to 38°N and from 117°E to 122°E, consisting of two provinces (Shandong and Jiangsu) and 44 counties and covering more than 64,000 km² (Fig. 1). The study area belongs to warm-temperate or subtropical climate zones and is located mostly between China's two longest rivers, the Yangtze and Yellow Rivers. Across different divisions within the study area, the coastline and land surface exhibit distinct spatial heterogeneities controlled by natural conditions and human activities. The divisions near the sides of the two rivers generally have muddy coasts due to the large amount of sediment input via the rivers^{8,39}, and wetlands are continuously distributed along the muddy coasts in forms of salt marshes such as the Yellow River Estuary (National Park) and Yancheng Coastal Wetlands (World Natural Heritage Site), containing huge potential of carbon sink^{40,41}. In contrast, rocky and sandy coasts are distributed over the remaining divisions. Additionally, humans exploit the coast and transform it into artificial

coasts by constructing docks, embankments, and ponds^{42,43}. The terrain is undulating in most divisions of Shandong Province, whereas it is generally flat over Jiangsu Province. Nearly every corner of the study area is occupied or altered by human activities. Croplands constitute the major landscape with mixed forests and grasslands, making large and different contributions to the soil carbon sink^{5,44}, and built-up areas are widely spread over the study area, with different types and intensities across divisions^{45,46}. During the last decade (from 2010 to 2020), ecological restoration projects that are featured by abundant connotations, various types, and extensive scope have been conducted in the study area; they covered nearly all forests, croplands, grasslands, wetlands, and built-up areas in aspects of scale control, spatial configuration, and quality promotion to enhance coastal ecosystem health^{47,48}. These circumstances render the study area suitable for mapping the spatiotemporal variations of large-scale coastal soil carbon stock in the context of extensive ecological restoration.

Here, in terms of field soil data, we obtained surface soil data in 2020 in 457 sites (Fig. 1) through field surveys, in-situ sampling, and laboratory measurements, while extracted those in 2010 at the same sites by referencing robust historical open source data⁴⁹. As for the predictors, we established a comprehensive land surface factor system (CLSFS)²², which consists of four aspects, namely, ecological indices, landscape composition, landscape configuration, and geographical position, and covers different types of natural and anthropogenic influencing factors; we extracted a total of 17 predictors based on open source remote sensing and land cover data. From the perspective of spatial resolution, we adopted 10 scales (simulation units) from fine (100 m) to coarse (1000 m) resolutions to determine the optimum resolution with high simulation accuracy and precise spatial details. We generated maps of surface soil organic carbon density (SOCD) in 2020 and 2010 and those of Δ SOC from 2010 to 2020 (SOCD in 2020 minus that in 2010) across the 10 scales. This study proposes the following hypothesis: Large-scale coastal surface soil carbon stock has increased remarkably and presents distinct spatial heterogeneities in northern China in the context of extensive ecological restoration. To validate this hypothesis, we must answer the following three scientific questions: (1) Which spatial resolution is optimal in coastal soil carbon mapping for high simulation accuracy and precise spatial details? (2) What are the main driving factors of spatiotemporal variations of coastal soil carbon stock in northern China during the last decade? (3) What are the effects of extensive ecological restoration on coastal soil carbon stock in the entire study area and across land cover types?

We found that the 100 m scale is the optimum resolution to map the large-scale coastal soil carbon stock for the good simulation accuracy and precise spatial details. Ecological quality promotion in the context of extensive ecological restoration was the main driving factor of the spatiotemporal variations in coastal soil carbon stock and increased the soil carbon stock to different degrees across land cover types.

Results and discussion

Simulation accuracies and spatial details across scales from 100 m to 1000 m. The simulation accuracies of soil organic carbon (SOC) across scales were measured using two commonly used metrics: root mean squared error (RMSE) and Lin's concordance correlation coefficient (Lin's CCC)^{50,51}, which refer to the absolute and relative errors, respectively, and a lower RMSE and higher Lin's CCC indicate higher simulation accuracy. The two metrics were calculated by comparing the simulated soil data with the field observed data in the validating samples and one value was generated for each of RMSE and Lin's CCC at one scale through a 10-fold cross-validation. The RMSE and Lin's CCC at a

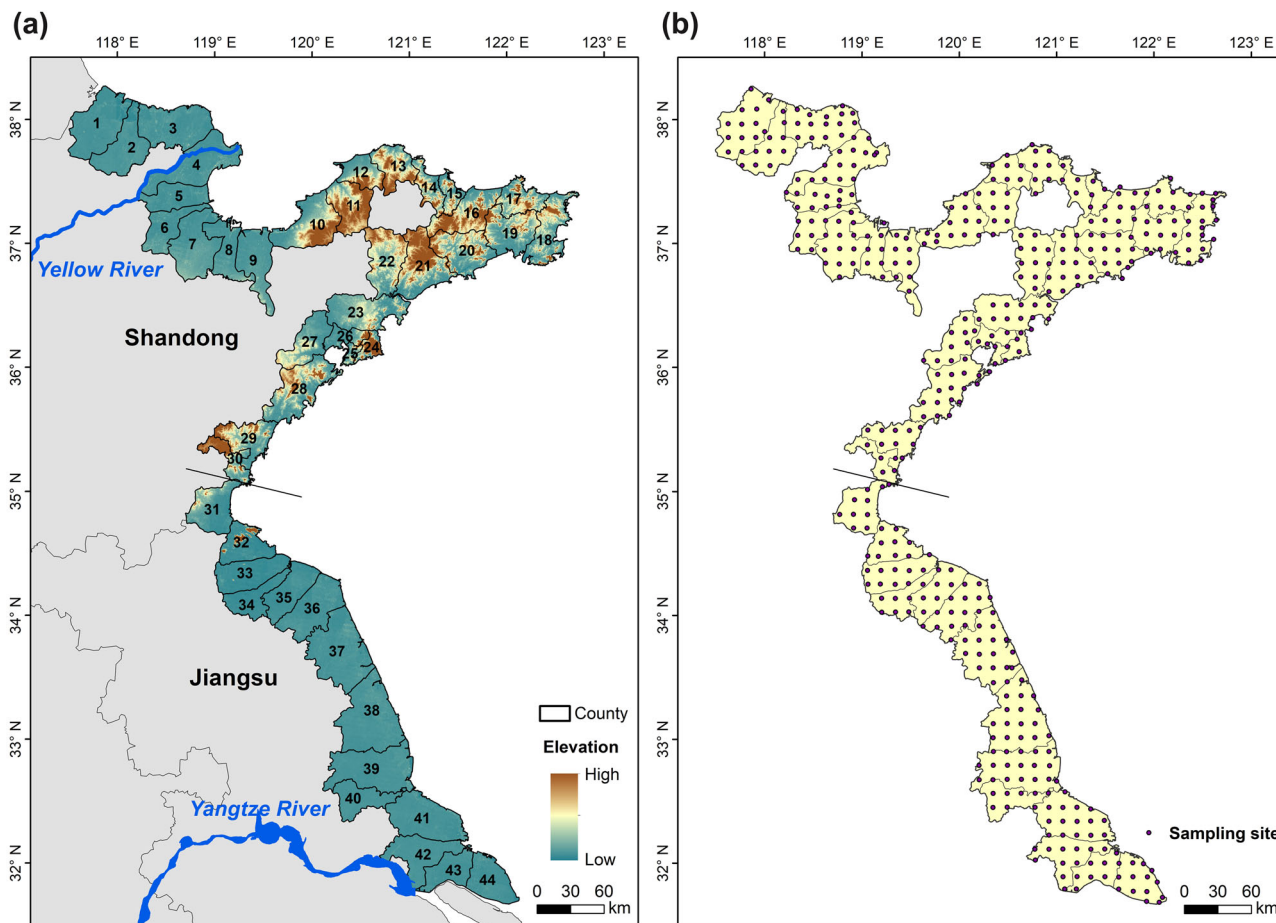


Fig. 1 Administrative divisions and sampling sites of the study area. **a** Administrative divisions. **b** Sampling sites. The oblique line is the boundary of Shandong Province (above) and Jiangsu Province (below). Counties 1–30 belong to Shandong Province while Counties 31–44 belong to Jiangsu Province. The detailed administrative divisions and their names can be referenced in Supplementary Table S1.

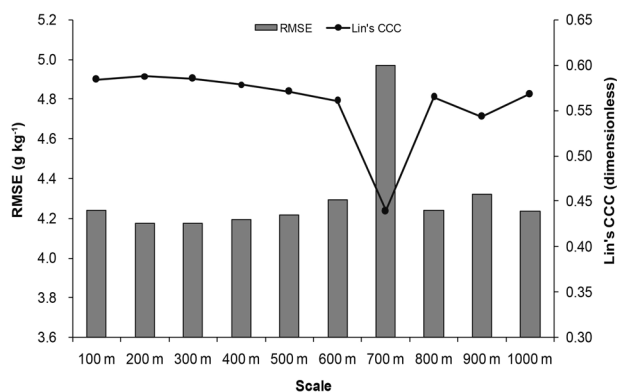


Fig. 2 Simulation accuracies of soil organic carbon (SOC) across scales from 100 m to 1000 m. RMSE root mean squared error, Lin's CCC Lin's concordance correlation coefficient.

scale represented the simulation accuracy at this scale (Fig. 2). The two metrics slightly fluctuated from 100 m to 500 m scales, with the highest accuracy achieved by the results at the 200 m scale; however, the difference among the five scales was small. At scales from 600 m to 1000 m, the simulation accuracy was generally lower than that at scales from 100 m to 500 m, and the 700 m scale presented the lowest accuracy among all the 10 scales. The RMSE from 100 m to 500 m scales was around 4.20 g kg^{-1} , which was higher than those in some cases at small spatial scales,

such as the Yellow River Delta in China (2.78 g kg^{-1})²², the southern tip of Liaodong Peninsula in China (2.79 g kg^{-1})⁵², and Erath and Comanche Counties in Texas in United States (4.10 g kg^{-1})⁵³, however, was much lower than those in studies at large scales, such as the whole Nigeria (6.75 g kg^{-1})⁵⁴, the whole China ($12.65\text{--}13.41 \text{ g kg}^{-1}$)^{27,55}, the whole Japanese forests (27.6 g kg^{-1})⁵⁶, and the whole Canada (58.60 g kg^{-1})⁵⁷. Lin's CCC from the 100 m to 500 m scales was higher than 0.55, which was in a high level compared with that reported in previous studies^{18,58,59}. This indicates that large-scale coastal surface soil carbon mapping in the present study achieved high simulation accuracy at a fine spatial resolution.

The maps of SOCD in 2020 and 2010 and those of Δ SOCD from 2010 to 2020 across scales from 100 m to 1000 m are presented in three extents to identify the spatial details (see Fig. 3 for maps of SOCD in 2020; see Supplementary Figs. S1 and S2 for maps of SOCD in 2010 and those of Δ SOCD from 2010 to 2020).

In Extent 1, which covers the entire study area, the map graininess was indistinct and the overall spatial characteristics of soil carbon were similar across the 10 scales. In Extent 2, which refers to County 4 (one of the 44 counties), the map graininess was indistinct from 100 m to 400 m scales, yet it became distinct at the 500 m scale and gradually increased from 500 m to 1000 m scales. In Extent 3, which indicates the mouth of the Yellow River (a specific geographical unit), all maps except that at the 100 m scale exhibited distinct graininess and graphically presented the differences from fine (100 m) to coarse (1000 m) spatial resolutions.

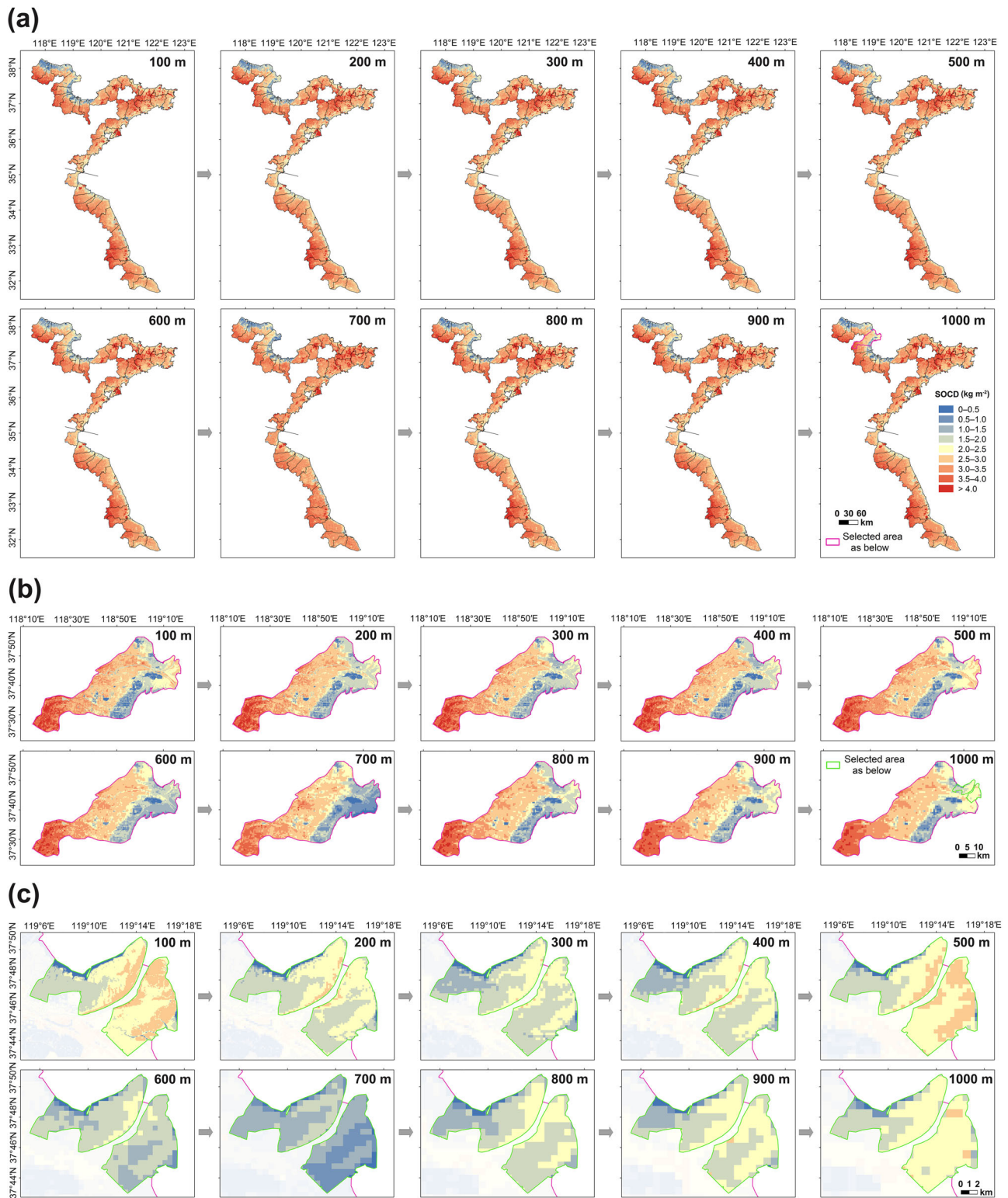


Fig. 3 Maps of soil organic carbon density (SOCD) in 2020 across scales from 100 m to 1000 m in the three extents. The scale refers to the minimum unit to conduct the SOC mapping, i.e., the spatial resolution of the maps. **a** Extent 1: the entire study area. **b** Extent 2: the selected area within Extent 1, i.e., Kenli District (County 4), Dongying City, Shandong Province. **c** Extent 3: the selected area within Extent 2, i.e., the mouth of the Yellow River.

The differences across scales were not only represented in graininess but also in the precision of the results (Fig. 4). The SOCD in 2020, Δ SOCD, soil organic carbon stock (SOCS) in 2020, and Δ SOCS (i.e., SOCS in 2020 minus that in 2010) fluctuated across the 10 scales in the three extents, yet the differences distinctly increased from Extent 1 to Extent 3. Particularly in Extent

3, Δ SOCD and Δ SOCS changed considerably across scales in aspects of quantity and quality (e.g., they were < 0 at 700 m scale). This result indicates that although the estimation of the soil carbon stock in the entire study area was generally similar across the 10 scales, the spatial details in a specific region, such as Extent 3, which is an important estuarine wetland and possesses huge

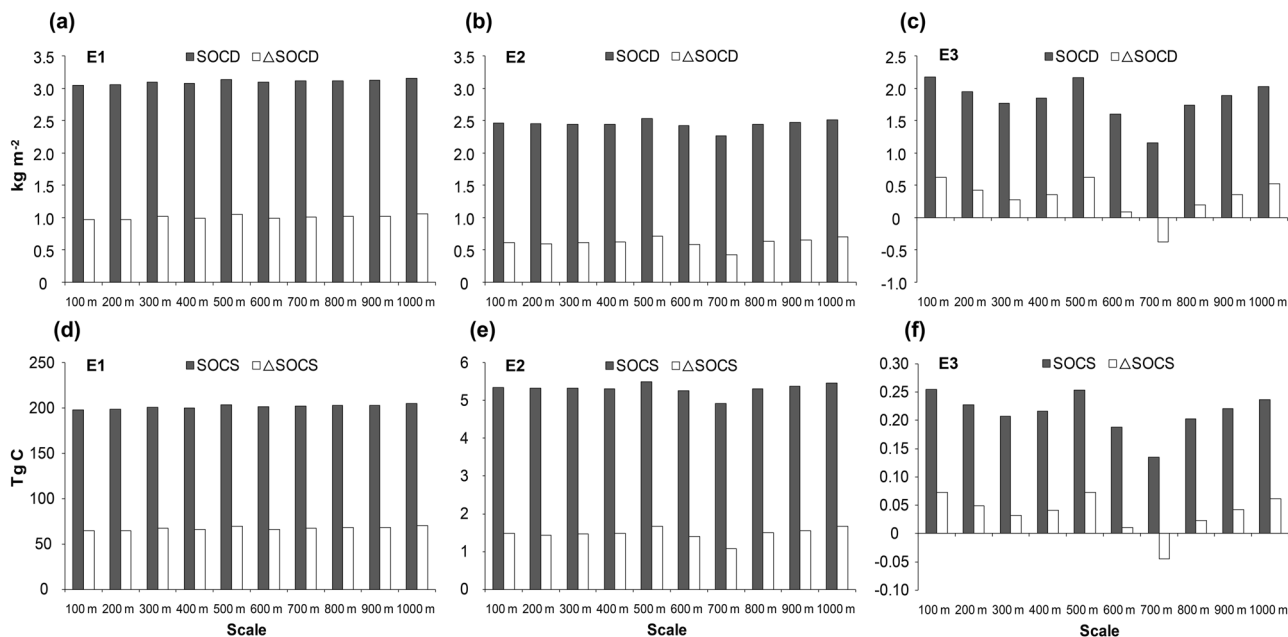


Fig. 4 Estimations of soil organic carbon density (SOCD) and stock (SOCS) across scales from 100 m to 1000 m in the three extents. E1, E2, and E3 refer to Extent 1, Extent 2, and Extent 3 presented in Fig. 3, respectively. SOCD/SOCS indicates that in 2020, i.e., $\text{SOCD}_{2020}/\text{SOCS}_{2020}$. $\Delta\text{SOCD}/\Delta\text{SOCS}$ indicates the SOCD/SOCS in 2020 minus that in 2010. **a** SOCD and ΔSOCD in Extent 1. **b** SOCD and ΔSOCD in Extent 2. **c** SOCD and ΔSOCD in Extent 3. **d** SOCS and ΔSOCS in Extent 1. **e** SOCS and ΔSOCS in Extent 2. **f** SOCS and ΔSOCS in Extent 3.

potential for blue carbon^{47,60}, might vary remarkably. Precise spatial details in a small extent greatly contribute to revealing the soil carbon stock in a specific geographic unit and improving the overall accuracy at a large scale^{28,29}.

In summary, good simulation accuracy was achieved at scales from 100 m to 500 m, of which the 100 m scale presented little map graininess in different extents and high precision in spatial details. Therefore, the scale of 100 m was recommended as the optimum spatial resolution to map the large-scale coastal soil carbon stock and was used to conduct the following studies, thereby answering the first scientific question of the study. The method for mapping the large-scale coastal soil carbon stock at a fine resolution is highly applicable in different areas for the easily accessible data source, clear and repeatable simulation process, and optimum spatial resolution. The needed data for the soil carbon mapping are field soil data and predictors. The former can be obtained through conventional field survey and sampling, along with applying for the inventory data, while the latter can be conveniently generated based on the open source remote sensing and land cover data by using the CLSFS. The simulation algorithm (partial least squares regression), validation approach (10-fold cross-validation), and accuracy metrics (RMSE and Lin's CCC) are all frequently used methods and possess clear procedure and high repeatability. The 100 m is recommended as the optimum spatial resolution for the high simulation accuracy and precise spatial details and can be applied to other studies on the large-scale coastal soil mapping. Further, the simulation unit in the method is in the vector form for calculating the predictors in aspects of landscape composition and fragmentation, thereby generating huge data amount (e.g., 6 534 950 simulation units in 2020) at the 100 m spatial resolution in the large-scale coastal areas and limiting the application at a larger scale. Under this circumstance, the 200 m spatial resolution can be adopted to balance the precision of the results and the data amount.

Spatiotemporal patterns of coastal soil carbon stock from 2010 to 2020. Coastal soil carbon stocks showed distinct spatio-temporal heterogeneity (Figs. 3, 5). In 2020, low SOCD areas were

always observed in the northwestern part of Shandong Province and the alongshore areas of Jiangsu Province, whereas high SOCD areas were generally distributed in the inland areas, particularly in the mountainous areas in Shandong Province and parts of the cropland in the two provinces (Fig. 3). The spatial pattern of ΔSOCD was in accordance with that of SOCD, that is, high SOCD areas always had high ΔSOCD . Most areas had $\Delta\text{SOCD} > 0$, indicating an overall increase in surface soil carbon stock in the entire study area; areas with $\Delta\text{SOCD} < 0$ were mainly distributed along the coastline (Fig. 5). In terms of different counties, the mean ΔSOCD in all counties was > 0 , yet the values distinctly varied across counties; the counties with high ΔSOCD were mostly located in the eastern part of Shandong Province; Counties 6, 16, and 24 achieved the highest three ΔSOCDs while Counties 3, 25, and 31 had the lowest three (Fig. 5).

The spatial patterns of SOCD and ΔSOCD were analyzed along latitudinal, longitudinal, and anthropogenic gradients. The latitudinal gradient is defined as the change in latitude from 31°N to 38°N in the study area. SOCD and ΔSOCD presented up-down-up-down trend with the increase in the latitude, and those in 38°N obtained much lower values than in the other latitudes (Fig. 6a). The longitudinal gradient refers to the change in the distance to the coastline (DTC) because China's continental coastline generally spreads from north to south⁶¹ and naturally forms a longitudinal gradient. The coastline is the most noteworthy boundary and undergoes a series of coastal processes, including sediment deposition and erosion⁶², storm surge⁶³, seawater intrusion⁶⁴, and soil salinization⁶⁵. SOCD and ΔSOCD consistently and gradually increased with the increase in DTC (Fig. 6b). The anthropogenic gradient was represented by the distance to built-up areas (DTB), which indicates the degree of anthropogenic interference with natural ecosystem⁶⁶. SOCD and ΔSOCD first increased and then decreased along the DTB gradient (Fig. 6c). The soil carbon storage and increment increased with the decrease in anthropogenic interference in areas with DTB < 2 km. These areas were covered mostly by croplands, built-up areas, forests, and grasslands, and SOCD and ΔSOCD increased through the conversation from

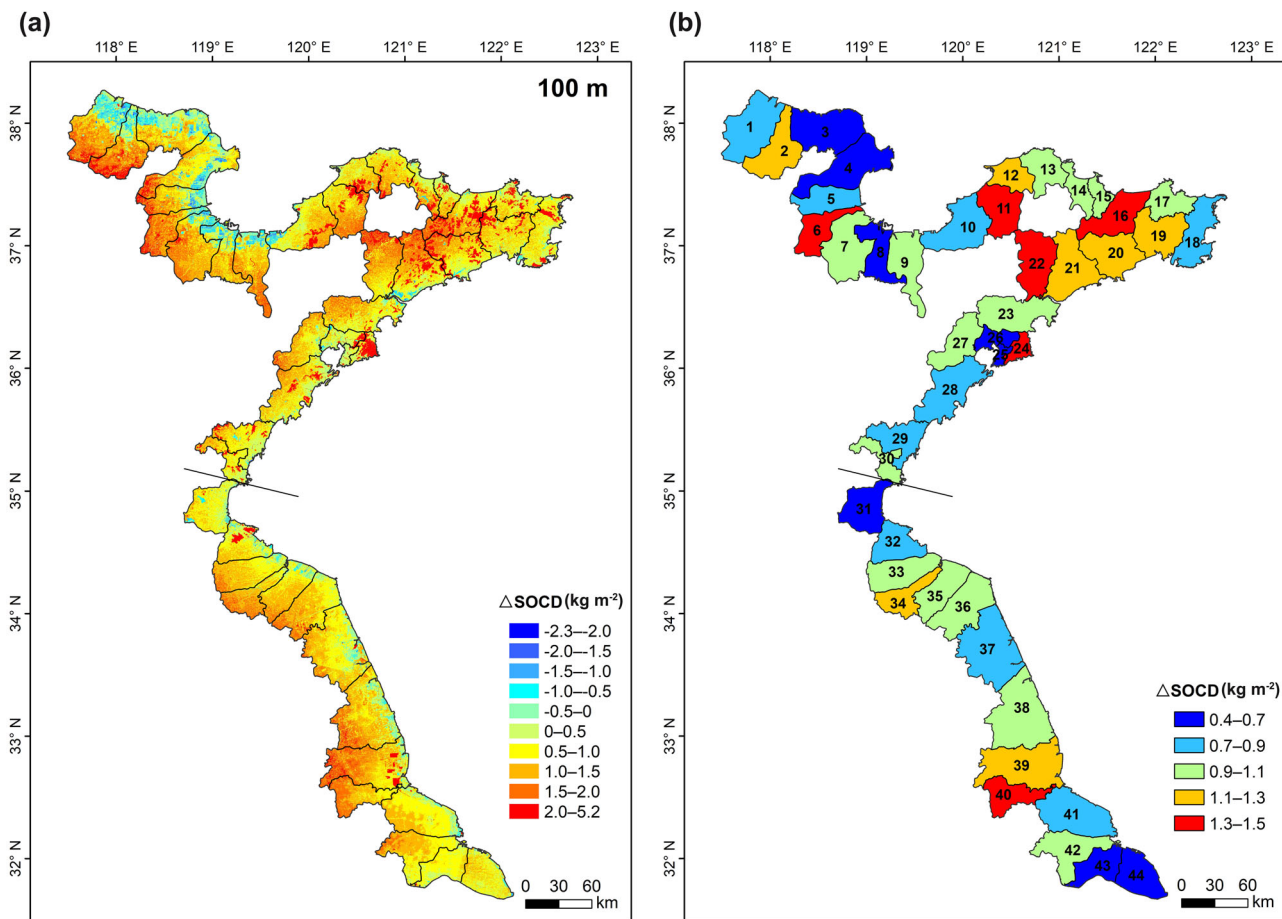


Fig. 5 Maps of Δ SOC D from 2010 to 2020. **a** Δ SOC D at the 100 m scale. **b** Δ SOC D in different counties. The names of Counties 1–44 can be referenced in Supplementary Table S1.

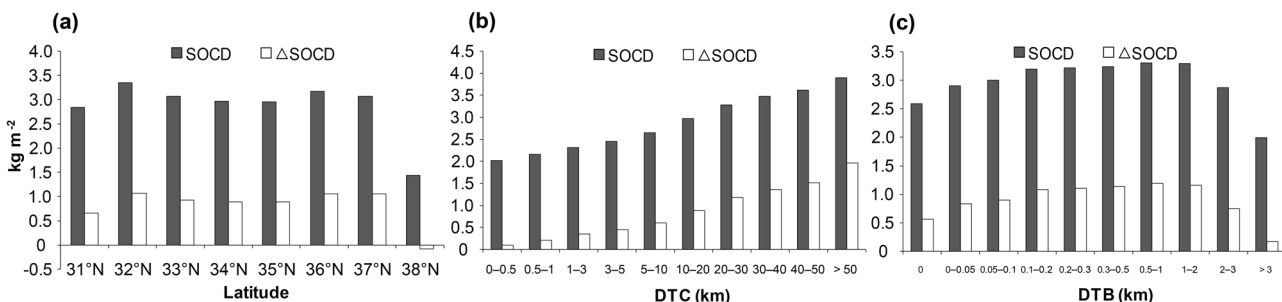


Fig. 6 Spatial patterns of SOC D and Δ SOC D along the multiple gradients. DTC distance to the coastline, DTB distance to built-up areas. **a** SOC D and Δ SOC D along the latitude gradient. **b** SOC D and Δ SOC D along the DTC gradient. **c** SOC D and Δ SOC D along the DTB gradient.

built-up areas to the other types. By contrast, the soil carbon storage and increment decreased with the increase in DTB in areas with DTB > 2 km. The DTB increase in these areas denoted the conversion from other land cover types to wetlands, thereby inducing the decrease in SOC D and Δ SOC D.

The predictors in the CLSFS constituted the potential influencing factors of the spatial pattern of coastal soil carbon stock, and their correlation coefficients with SOC D and Δ SOC D varied remarkably across predictors (Table 1).

The predictors include four aspects: ecological indices, landscape composition, landscape configuration, and geographical position. The ecological indices directly represent the vegetation growth condition and ecological quality^{67,68}; they had distinctly higher correlations with SOC D and Δ SOC D than the remaining

three aspects. It denoted that the ecological quality determined the spatial pattern of SOC D and the quality promotion dominated the spatiotemporal variation of coastal soil carbon stock, that is, areas with good ecological quality always had high SOC D and those with large quality promotion generally exhibited high Δ SOC D. Landscape composition refers to the area proportions of different land cover types and generally influences soil carbon by determining the vegetation types and underlying surface^{69,70}. The predictors of landscape composition had distinct correlations with SOC D; SOC D was high in vegetation areas and croplands but low in wetlands and built-up areas. In contrast, they exhibited weak correlations with Δ SOC D, indicating that the change in land cover types was not the main factor driving the spatiotemporal variations of coastal soil carbon stock during the

Table 1 Correlation coefficients of soil organic carbon density (SOCD) with the potential influencing factors.

Items		SOC D	ΔSOC D
Ecological indices	DVI/ΔDVI	0.693	0.342
	NDVI/ΔNDVI	0.796	0.408
	SAVI/ΔSAVI	0.740	0.370
Landscape composition	VC/ΔVC	0.241	0.107
	FP/ΔFP	0.390	0.142
	GP/ΔGP	0.366	0.146
	CP/ΔCP	0.338	0.014
	WP/ΔWP	-0.252	-0.019
	BP/ΔBP	-0.199	-0.135
	WAP/ΔWAP	-0.534	-0.049
Landscape configuration	NP/ΔNP	0.048	-0.066
	TE/ΔTE	0.093	-0.05
	AWMSI/ΔAWMSI	0.041	-0.114
	SWI/ΔSWI	0.065	0.039
	LII/ΔLII	-0.132	-0.132
Geographical position	DTC/ΔDTC	0.508	0.165
	DTB/ΔDTB	-0.228	0.273
EI		0.420	0.435
SI		0.362	0.364

The correlations were conducted using the results at the 100 m scale through Minitab. The correlation coefficient indicates the Pearson correlation coefficient; $n = 6534\ 387$ for SOCD and $6542\ 596$ for ΔSOCD; $p < 0.01$ for all the correlations. SOCD is the SOCD in 2020; ΔSOCD is the SOCD in 2020 minus that in 2010. The same situations apply to the influencing factors, e.g., DVI is the DVI in 2020 while ΔDVI is the DVI in 2020 minus that in 2010. DVI difference vegetation index, dimensionless, NDVI normalized difference vegetation index, dimensionless, SAVI soil adjusted vegetation index, dimensionless, VC vegetation coverage, %, FP forest proportion, %, GP grassland proportion, %, CP cropland proportion, %, WP wetland proportion, %, BP built-up area proportion, %, WAP water area proportion, %, NP number of patches, ind., TE total edges, m, AWMSI area-weighted mean shape index, dimensionless, SWI Shannon-Wiener index, dimensionless, LII landscape isolation index, dimensionless, DTC distance to the coastline, km, DTB distance to built-up areas, km., EI elevation, m, SI slope, °.

last decade. The study area is a highly developed area with intensive land use for a long term, and land cover changes of different types have generally been small during the last decade⁷¹ under the policies of ecological civilization⁷² and farmland protection⁷³. Landscape configuration indicates the spatial arrangement and positional interrelations of landscape patches and is characterized by fragmentation driven by human activities in coastal areas^{74,75}. The predictors in landscape configuration presented low correlations with SOCD and ΔSOCD, denoting the small contribution of landscape fragmentation to the spatiotemporal patterns of coastal soil carbon stock at the large scale. This result is not in accordance with those of previous studies conducted at the local scale^{37,76}. It can be inferred that the effect of landscape fragmentation on soil carbon may decrease with the increase in scale. For the geographical position, DTC exhibited a positive and high correlation with SOCD, which corresponded to the result in Fig. 6, but a low one with ΔSOCD. DTC influenced the soil carbon stock in the entire study area mainly by influencing the spatial pattern of land surface characteristics. The effect of coastline evolution caused by natural processes and anthropogenic intervention on soil carbon variation was distinct in alongshore areas. DTB was negatively correlated with SOCD but positively correlated with ΔSOCD. This indicates that human activities could contribute to an increase in soil carbon when the interference was low (e.g., farming and plantation), but led to a decrease in soil carbon when the interference increased (e.g., urbanization)^{77,78}. Besides the predictors, two terrain factors, namely, elevation and slope, were used to identify the spatial pattern of coastal soil carbon stock, and had positive and high correlations with SOCD and ΔSOCD. Mountainous areas showed higher soil carbon stock and larger increase in stock than flat areas because mountainous areas are mostly covered by forests

and grasslands⁷¹, which possessed high SOCD and ΔSOCD in the context of ecological restoration.

Therefore, ecological quality promotion in the context of extensive ecological restoration was the main driving factor of the spatiotemporal variations in coastal soil carbon stock at the large scale, and coastline evolution controlled by natural and anthropogenic processes considerably influenced the soil carbon stock in the alongshore areas. These results answer the second scientific question.

Effects of extensive ecological restoration on coastal carbon soil stock. Based on the high-resolution maps of coastal soil carbon stock at the 100 m scale, the total amount of surface SOCS in the entire area in 2020 summed to 197.80 Tg C, increasing by 39.19 % from 2010 to 2020, and the mean value of surface SOCD was 3.04 kg m⁻², increasing by 37.82 % from 2010 to 2020.

As illustrated earlier, the increase in coastal soil carbon stock is mostly attributed to the quality promotion of coastal ecosystems in the context of extensive ecological restoration that cover the entire study area. Within the study area, different types of ecological restoration projects cover the land surface and correspond to different land cover types, including forests, grasslands, croplands, wetlands, and built-up areas¹⁶. All the types are closely related and form a multi-component community of life⁷⁹, in which the soil serves as the basis for humans: The soil supports the vegetation in different land cover types, thereby providing essential ecological, productive, and recreational functions for human survival and sustainable development. The ΔSOCDs of the five land cover types were all >0, indicating the positive effects of different types of ecological restoration on the coastal soil carbon stock; forests, grasslands, croplands, built-up areas, and wetlands were in descending order of SOCD and ΔSOCD, and the differences among land cover types were large (Fig. 7a). In terms of the total amount of SOCS, croplands occupied the most because of its large area and its ΔSOCS contributed the most, followed by built-up areas, which covered a considerable part (Fig. 7b). From the perspective of the increase rates from 2010 to 2020 (Fig. 7c), the increase rate of SOCD in the entire study area was slightly lower than that of SOCS because the natural increase in coastal wetlands and anthropogenic sea reclamation enlarged the study area from 2010 to 2020. For the five land cover types, the difference in the increase rate between the SOCD and SOCS was attributed to area changes. Specifically, areas of forests, wetlands, and built-up areas increased, while those of grasslands and croplands decreased, resulting in the higher increase rate in SOCS than that in SOCD for forests, wetlands, and built-up areas, but the lower increase rate in SOCS than that in SOCD for grasslands and croplands. Considering that the area increase in certain land covers was not the outcome of ecological restoration (e.g., the increase in built-up areas was due largely to urbanization), the increase rates of SOCD were adopted to identify the effects of different types of ecological restoration on coastal soil carbon stock; the SOCDs of forests, grasslands, croplands, wetlands, and built-up areas increased by 72.58%, 74.25%, 41.39%, 4.58%, and 26.30%, respectively, from 2010 to 2020 in the context of extensive ecological restoration. This corresponds to the third scientific question of this study.

During the last decade, extensive ecological restoration projects have been implemented for multiple components of the community. For forests and grasslands, new plantations were established in barren mountains and lands, and replantation was carried out in degraded forests and grasslands by mainly adopting native species and jointly considering the tree, shrub, and herb layers to ensure the vegetation scale, thereby increasing the areas of forests and inevitably decreasing those of grasslands in the study area. Vegetation quality was promoted in the following two aspects:

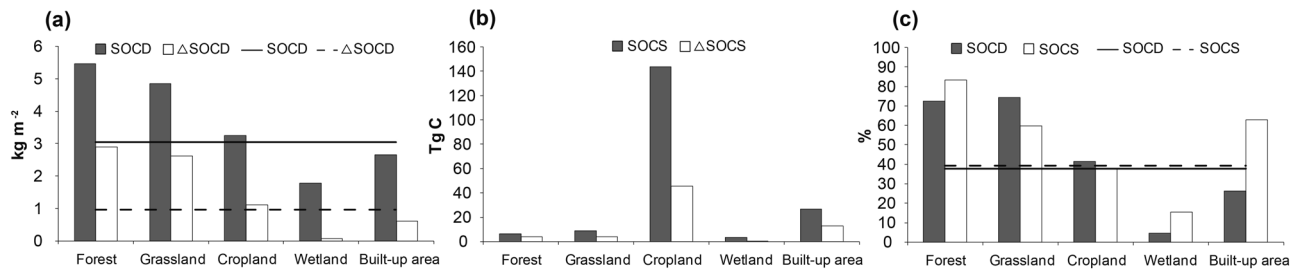


Fig. 7 Effects of extensive ecological restoration on coastal soil carbon stock. **a** The columns indicate SOCD and Δ SOCD across land cover types while the solid and dashed lines refer to the mean values of SOCD and Δ SOCD in the entire study area, respectively. **b** The columns indicate SOCS and Δ SOCS across land cover types. **c** The columns indicate the increase rates of SOCD and SOCS from 2010 to 2020 across land cover types while the solid and dashed lines refer to the mean values of increase rates of SOCD and SOCS from 2010 to 2020 in the entire study area, respectively.

First, natural and secondary forests, particularly young growth, were strictly protected; second, plantations were progressively enhanced by nurturing multi-layer and uneven-aged forest stands and optimizing tree species structure, especially in coastal shelter forests⁵. The self-restoring capacity of grasslands has been used to improve the ecological quality, accompanying with the forest restoration. In addition, forest fires were cautiously and routinely prevented to minimize the carbon emissions resulting from the fire, and a special project was conducted to control invasive species, especially *Bursaphelenchus xylophilus*, which has wreaked havoc on pine forests in China's coastal areas⁸⁰. Correspondingly, the soil carbon stocks of forests and grasslands have increased remarkably in the study area. For croplands, high-standard ones were constructed to pursue the goal of integration of quantity and quality, and a series of tillage practice^{81,82}, including straw return, organic fertilizer and green manure application, no (or minimum) tillage, land use and maintenance combination, and cropland shelterbelt construction, were conducted to increase the soil carbon stock. Wetlands have been protected mainly through natural processes, in which areas of coastal wetlands have increased during the last decade. In the damaged wetlands, specific projects such as Blue Bay Remediation Project and Coastal Protection and Restoration Project were implemented to recover the damaged wetlands and improve the vegetation scale and quality in salt marshes⁸³. The wetland SOCS distinctly increased because of the expansion of coastal wetlands; the newly formed coastal wetlands always had low SOCD (see Extent 3 in Fig. 3), thus Δ SOCD of wetlands was generally low. In built-up areas, spatial resources were adequately utilized based on land spatial planning⁸⁴ to establish the green space system through the Urban Ecological Restoration Project to increase the scale and connectivity of green spaces and improve the soil carbon stock.

Therefore, coastal surface soil carbon stock in northern China has remarkably increased from 2010 to 2020 in the context of extensive ecological restoration and SOCD and Δ SOCD exhibited distinct spatiotemporal heterogeneities in different administrative divisions, along the multiple gradients, and across land cover types. This validated the study's hypotheses.

Methods

Data acquisition. Field soil data: Field data in 2020 were obtained from a large-scale field survey. The sampling sites were set following a grid sampling pattern⁸⁵, that is, the sites were evenly distributed within the study area and one site was set every 12.5 km to balance the comprehensiveness and cost. In the process of field investigation, the factual positions of sampling sites were adjusted in the consideration of representativeness and accessibility: The factual site should represent the ecological characteristics of the

surrounding areas and can be easily reached to ensure the successive investigation. Finally, a total of 457 sites were surveyed (see Fig. 1). The surface (0–20 cm) soil was sampled and soil factors were measured in the laboratory. Bulk density (BD) was measured using a cutting ring with a volume of 100 cm³ and SOC was measured using the potassium dichromate oxidation method. Field data in 2010 were collected from the National Earth System Science Data Center, National Science & Technology Infrastructure of China (<https://www.geodata.cn>). Soil data in the same sites to 2020 were extracted to ensure spatial consistency of the sites across the two time points, and the data in 438 sites were available for 2010 because of the coastline evolution from 2010 to 2020. The field soil data are presented in Supplementary Table S2. In the field soil data, the mean values of SOC were 11.77 g kg⁻¹ and 7.98 g kg⁻¹ in 2020 and 2010, respectively; those in forests, grasslands, croplands, wetlands, and built-up areas were 22.86 g kg⁻¹, 19.12 g kg⁻¹, 11.65 g kg⁻¹, 6.41 g kg⁻¹, and 9.89 g kg⁻¹ in 2020, respectively, and were 9.64 g kg⁻¹, 8.57 g kg⁻¹, 8.01 g kg⁻¹, 5.92 g kg⁻¹, 8.21 g kg⁻¹ in 2010, respectively.

Remote sensing data: Data from Landsat satellites were adopted; data in 2020 were from Landsat 8 and those in 2010 were from Landsat 5 to ensure temporal consistency between field and remote sensing data, and the multi-spectral bands had a spatial resolution of 30 m. At each of the two time points, remote sensing images that covered the entire study area, had little or no clouds (cloud cover ranged from 0 to 4%), and possessed temporal consistency across images were collected. The information of the Landsat data are presented in Supplementary Table S3. The spectral reflectance map for each band at each time point was generated through radiometric calibration and atmospheric correction. In addition, the coastline of the study area in 2020 and 2010 was extracted based on remote sensing images that fused different bands to exhibit RGB color. The extent of the study area containing administrative divisions was then determined (see Fig. 1).

Land cover data: Open-source land cover data were collected from GlobeLand30 (www.globallandcover.com). The data were extracted mainly from Landsat and Chinese HJ-1 and GF-1 satellite images and had good classification accuracy⁸⁶ with overall accuracies of 83.50% and 85.72% for 2010 and 2020, respectively, and kappa coefficients of 0.78 and 0.82, respectively. The data had a spatial resolution of 30 m, thereby ensuring spatial consistency with the aforementioned multispectral remote sensing data. According to GlobeLand30 data, land cover in the study area can be classified into seven types: forests, grasslands, croplands, wetlands, built-up areas, water areas, and bare lands (see Supplementary Fig. S3). The cropland was the landscape matrix, covering more than 65% of the entire study area, but its area slightly decreased from 2010 to 2020; in contrast, the proportion of built-up areas increased from 10.80% to 15.65% from 2010 to 2020; forests and grasslands were generally

distributed in the mountainous areas and in the upland along the coastline; wetlands were mostly located in the alongshore areas in the form of salt marshes; water areas consisted of natural rivers and lakes, as well as artificial ponds; and bare lands presented a very small proportion and were scattered within the study area.

In summary, the multi-source data ensured spatial consistency in field soil data across the two time points and between the remote sensing and land cover data, as well as temporal consistency among the field, remote sensing, and land cover data, thereby meeting the demand for high-resolution coastal soil carbon mapping at a large scale.

Predictors in CLSFS. The predictors were selected followed the CLSFS²², which is characterized by comprehensiveness and applicability. Comprehensiveness is realized by the 17 predictors in the four aspects that cover different dimensions of potential influencing factors of soil carbon, and applicability denotes that all predictors are sourced from the open source remote sensing and land cover data.

Ecological indices: Three predictors, difference vegetation index (DVI), normalized difference vegetation index (NDVI), and soil-adjusted vegetation index (SAVI), were selected. The equations used are as follows^{87,88}:

$$DVI = Re_5 - Re_4 \tag{1}$$

$$NDVI = \frac{Re_5 - Re_4}{Re_5 + Re_4} \tag{2}$$

$$SAVI = \frac{Re_5 - Re_4}{Re_5 + Re_4 + L} \times (1 + L) \tag{3}$$

where Re_x is the spectral reflectance of B_x for Landsat 8 data in 2020 and should be minus one (i.e., B_{x-1}) for Landsat 5 data in 2010; L is given as 0.5.

Landscape composition: The following seven predictors were used: vegetation coverage (VC), forest proportion (FP), grassland proportion (GP), cropland proportion (CP), wetland proportion (WP), built-up area proportion (BP), and water area proportion (WAP). The equations were proposed in the study as follows:

$$VC = \frac{FA + GA + WA}{TA} \times 100\% \tag{4}$$

$$FP = \frac{FA}{TA} \times 100\% \tag{5}$$

$$GP = \frac{GA}{TA} \times 100\% \tag{6}$$

$$CP = \frac{CA}{TA} \times 100\% \tag{7}$$

$$WP = \frac{WA}{TA} \times 100\% \tag{8}$$

$$BP = \frac{BA}{TA} \times 100\% \tag{9}$$

$$WAP = \frac{WAA}{TA} \times 100\% \tag{10}$$

where FA, GA, WA, CA, BA, and WAA are the areas of forests, grasslands, wetlands, croplands, built-up areas, and water areas, respectively, and TA is the total area of the simulation unit.

Landscape configuration: Five predictors, including number of patches (NP), total edges (TE), area-weighted mean shape index (AWMSI), Shannon-Wiener index (SWI), and landscape isolation index (LII), were selected. NP and TE were directly measured using the total number and perimeter of patches in the simulation unit,

respectively. The equations for the three remaining predictors are as follows⁸⁹:

$$AWMSI = \sum \left(\frac{0.25 \times LP_i}{\sqrt{LA_i}} \times \frac{LA_i}{TA} \right) \tag{11}$$

$$SWI = -\sum \left[\frac{LA_i}{TA} \times \ln \left(\frac{LA_i}{TA} \right) \right] \tag{12}$$

$$LII = \sum \left(0.5 \times \sqrt{\frac{LN_i}{TA}} \times \frac{TA}{LA_i} \right) \tag{13}$$

where LP_i , LA_i , and LN_i are the perimeter, area, and number of landscape type i , respectively.

Geographical position: Two predictors, distance to the coastline (DTC) and distance to built-up areas (DTB), were used. These values were calculated by entering the vector data of coastline and built-up areas into the *Euclidean Distance* tool in ArcGIS.

Therefore, 17 predictors in the four aspects were obtained based on the open source remote sensing and land cover data (see Supplementary Figs. S4–S20).

Spatial simulations across scales. Ten scales (the scale here indicates the spatial resolution to conduct the simulation, i.e., the simulation unit) from 100 m to 1000 m (from fine to coarse resolutions) were used to determine the optimum scale for achieving high simulation accuracy and precise spatial details. Simulation units at the 10 scales were generated using the *Fishnet* tool in ArcGIS. The numbers of simulation units from 100 m to 1000 m in 2020 summed to 6 534 950, 1 642 362, 733 594, 414 710, 266 648, 186 050, 137 341, 105 616, 838 00, and 68 199, respectively, while those in 2010 summed to 6 441 180, 1 618 441, 722 864, 408 519, 262 659, 183 245, 135 267, 103 986, 82 530, and 67 145, respectively. Seventeen predictors were spatially exhibited based on the 10 scales, and 10 maps were produced for each predictor at each time point. A total of 340 maps for the 17 predictors across the two time points are presented in Supplementary Figs. S4–S20.

At each of the 10 scales, the 10-fold cross-validation method was used to conduct the spatial simulation and validate the simulation accuracy and uncertainty. Specifically, the field soil data from the 457 sites were randomly and evenly divided into 10 groups. Each of the 10 groups was considered validating samples, while the remaining nine groups were considered training samples, with every group serving as the validating samples once. A commonly used algorithm, namely, partial least squares regression, was used to implement the simulations through Minitab Statistical Software v20 to ensure repeatability. Thus, 10 sets of results were obtained at a scale, and the mean value and standard deviation of the 10 sets were used as the final simulation result and uncertainty at the scale (see Supplementary Figs. S21–S24). The simulation accuracies across the scales were measured using the RMSE and Lin's CCC, and the equations are as follows^{90,91}:

$$RMSE = \sqrt{\frac{1}{n} \sum_{i=1}^n (SV_i - OV_i)^2} \tag{14}$$

$$Lin's\ CCC = \frac{2CC \times SD_s \times SD_o}{(MV_s - MV_o)^2 + SD_s^2 + SD_o^2} \tag{15}$$

where SV_i and OV_i are the simulated and observed values in validating sample i , respectively; CC is the correlation coefficient between the simulated and observed values; SD_s and SD_o are the standard deviations of the simulated and observed values, respectively; and MV_s and MV_o are the mean simulated and

observed values, respectively. The simulated values at the 457 sites across the 10 scales through the 10-fold cross-validation are presented in Supplementary Table S4.

Effects of ecological restoration on coastal soil carbon. Maps of SOCD in 2020 and 2010 and those of Δ SOCD from 2010 to 2020 were generated based on spatial simulations across scales; the maps using the 10 spatial resolutions are presented in Fig. 3 and Supplementary Figs. S1 and S2. Owing to the large scale of the study area and limited map size, three extents of maps were presented to exhibit spatial details at different scales to determine the optimum scale. Extents 1, 2, and 3 are the entire study area, Kenli District, and the mouth of the Yellow River, respectively, and refer to large, intermediate, and small scales, respectively.

The spatial resolution with high simulation accuracy and precise spatial details was used as the optimum resolution to analyze the spatiotemporal patterns of SOCD in 2020 and Δ SOCD from 2010 to 2020 in the entire study and along multiple scales. The SOCS in 2020 and Δ SOCS from 2010 to 2020 were estimated based on the corresponding SOCD maps at the optimum scale. Thus, the effects of extensive ecological restoration on coastal soil carbon over the entire study area were identified. Then, SOCD, Δ SOCD, SOCS, and Δ SOCS for the five main land cover types, namely, forests, grasslands, croplands, wetlands, and built-up areas, were assessed to correspond to different types of ecological restoration, and the effects of different types of ecological restoration on coastal soil carbon were identified. Though built-up areas were characterized by the impervious surface in most areas, vegetation and bare soils could be observed mixed in them because of the mixed pixel of remote sensing data, and the circumstance was common and acceptable in regional ecological research^{92,93}. Besides, the size of simulation unit is 100 m \times 100 m, which may contain multiple land cover types.

Data availability

The source data that underlie all the figures in this study have been deposited in the Figshare database (<https://doi.org/10.6084/m9.figshare.24187368>). The field soil data in the 457 sites is provided in Supplementary Table S2; the remote sensing data used in this study are available from USGS (<https://glovis.usgs.gov/>) and the detailed information is presented in Supplementary Table S3; the land cover data used in this study are available from GlobeLand30 (www.globallandcover.com).

Received: 24 June 2023; Accepted: 4 October 2023;

Published online: 13 October 2023

References

- Xiang, D., Wang, G., Tian, J. & Li, W. Global patterns and edaphic-climatic controls of soil carbon decomposition kinetics predicted from incubation experiments. *Nat. Commun.* **14**, 2171 (2023).
- McBratney, A., Field, D. J. & Koch, A. The dimensions of soil security. *Geoderma* **213**, 203–213 (2014).
- Duarte, C., Losada, I., Hendriks, I., Mazarrasa, I. & Marbà, N. The role of coastal plant communities for climate change mitigation and adaptation. *Nat. Clim. Change* **3**, 961–968 (2013).
- Serrano, O. et al. Australian vegetated coastal ecosystems as global hotspots for climate change mitigation. *Nat. Commun.* **10**, 4313 (2019).
- Li, Y. et al. An overlooked soil carbon pool in vegetated coastal ecosystems: National-scale assessment of soil organic carbon stocks in coastal shelter forests of China. *Sci. Total Environ.* **876**, 162823 (2023).
- Haywood, B. J., Hayes, M. P., White, J. R. & Cook, R. L. Potential fate of wetland soil carbon in a deltaic coastal wetland subjected to high relative sea level rise. *Sci. Total Environ.* **711**, 135185 (2020).
- Gao, Y. et al. New insight into global blue carbon estimation under human activity in land-sea interaction area: a case study of China. *Earth-Sci. Rev.* **159**, 36–46 (2016).
- Li, X., Zhou, Y., Zhang, L. & Kuang, R. Shoreline change of Chongming Dongtan and response to river sediment load: a remote sensing assessment. *J. Hydrol.* **511**, 432–442 (2014).
- Sapkota, Y. & White, J. R. Long-term fate of rapidly eroding carbon stock soil profiles in coastal wetlands. *Sci. Total Environ.* **753**, 141913 (2021).
- Bu, N. et al. Reclamation of coastal salt marshes promoted carbon loss from previously-sequestered soil carbon pool. *Ecol. Eng.* **81**, 335–339 (2015).
- Yu, J. et al. Soil organic carbon storage changes in coastal wetlands of the modern Yellow River Delta from 2000 to 2009. *Biogeosciences* **9**, 2325–2331 (2012).
- Richards, D. R., Thompson, B. S. & Wijedasa, L. Quantifying net loss of global mangrove carbon stocks from 20 years of land cover change. *Nat. Commun.* **11**, 4260 (2020).
- Bryan, B. A. et al. China's response to a national land-system sustainability emergency. *Nature* **559**, 193–204 (2018).
- Wang, X. et al. Rebound in China's coastal wetlands following conservation and restoration. *Nat. Sustain.* **4**, 1076–1083 (2021).
- Song, W., Feng, Y. & Wang, Z. Ecological restoration programs dominate vegetation greening in China. *Sci. Total Environ.* **848**, 157729 (2022).
- Chen, X. et al. Distribution of ecological restoration projects associated with land use and land cover change in China and their ecological impacts. *Sci. Total Environ.* **825**, 153938 (2022).
- Yang, Y., Tilman, D., Furey, G. & Lehman, C. Soil carbon sequestration accelerated by restoration of grassland biodiversity. *Nat. Commun.* **10**, 718 (2019).
- Chi, Y., Sun, J., Liu, D. & Xie, Z. Reconstructions of four-dimensional spatiotemporal characteristics of soil organic carbon stock in coastal wetlands during the last decades. *Catena* **218**, 106553 (2022).
- Arrouays, D. et al. Soil legacy data rescue via GlobalSoilMap and other international and national initiatives. *GeoResJ* **14**, 1–19 (2017).
- Grinand, C. et al. Estimating temporal changes in soil carbon stocks at ecoregional scale in Madagascar using remote-sensing. *Int. J. Appl. Earth Obs.* **54**, 1–14 (2017).
- Fatholoumi, S. et al. Improved digital soil mapping with multitemporal remotely sensed satellite data fusion: a case study in Iran. *Sci. Total Environ.* **721**, 137703 (2020).
- Chi, Y., Shi, H., Zheng, W. & Sun, J. Simulating spatial distribution of coastal soil carbon content using a comprehensive land surface factor system based on remote sensing. *Sci. Total Environ.* **628–629**, 384–399 (2018).
- Saurette, D. D. et al. Effects of sample size and covariate resolution on field-scale predictive digital mapping of soil carbon. *Geoderma* **425**, 116054 (2022).
- Liang, Z. et al. National digital soil map of organic matter in topsoil and its associated uncertainty in 1980's China. *Geoderma* **335**, 47–56 (2019).
- Yang et al. The effectiveness of digital soil mapping with temporal variables in modeling soil organic carbon changes. *Geoderma* **405**, 115407 (2022).
- Shangguan et al. A China data set of soil properties for land surface modeling. *J. Adv. Model. Earth Syst.* **5**, 212–224 (2013).
- Li, Q. et al. Spatially distributed modeling of soil organic matter across China: an application of artificial neural network approach. *Catena* **104**, 210–218 (2013).
- Vitharana, U. W. A., Mishra, U. & Mapa, R. B. National soil organic carbon estimates can improve global estimates. *Geoderma* **337**, 55–64 (2019).
- Hengl, T. et al. African soil properties and nutrients mapped at 30 m spatial resolution using two-scale ensemble machine learning. *Sci. Rep.* **11**, 1–18 (2021).
- Walden, L. et al. Multi-scale mapping of Australia's terrestrial and blue carbon stocks and their continental and bioregional drivers. *Commun. Earth Environ.* **4**, 189 (2023).
- Hamzhepour, N. & Bogaert, P. Improved spatiotemporal monitoring of soil salinity using filtered kriging with measurement errors: an application to the West Urmia Lake. Iran. *Geoderma* **295**, 22–33 (2017).
- Khaledian, Y. & Miller, B. A. Selecting appropriate machine learning methods for digital soil mapping. *Appl. Math. Model.* **81**, 401–418 (2020).
- Chen, S. et al. Integrating additional spectroscopically inferred soil data improves the accuracy of digital soil mapping. *Geoderma* **433**, 116467 (2023).
- Long, J. et al. Effects of sampling density on interpolation accuracy for farmland soil organic matter concentration in a large region of complex topography. *Ecol. Indic.* **93**, 562–571 (2018).
- Miller, B. A., Koszinski, S., Wehrhan, M. & Sommer, M. Impact of multi-scale predictor selection for modeling soil properties. *Geoderma* **239–240**, 97–106 (2015).
- Pahlavan-Rad, M. R. et al. Legacy soil maps as a covariate in digital soil mapping: a case study from Northern Iran. *Geoderma* **279**, 141–148 (2016).
- Chi, Y., Zhao, M., Sun, J., Xie, Z. & Wang, E. Mapping soil total nitrogen in an estuarine area with high landscape fragmentation using a multiple-scale approach. *Geoderma* **339**, 70–84 (2019).
- Zhou, T. et al. Mapping soil organic carbon content using multi-source remote sensing variables in the Heihe River Basin in China. *Ecol. Indic.* **114**, 106288 (2020).

39. Kong, D. et al. Evolution of the Yellow River Delta and its relationship with runoff and sediment load from 1983 to 2011. *J. Hydrol.* **520**, 157–167 (2015).
40. Mao, D. et al. National wetland mapping in China: a new product resulting from object-based and hierarchical classification of Landsat 8 OLI images. *ISPRS J. Photogramm.* **164**, 11–25 (2020).
41. Zhang, S., Tian, J., Lu, X. & Tian, Q. Temporal and spatial dynamics distribution of organic carbon content of surface soil in coastal wetlands of Yancheng, China from 2000 to 2022 based on Landsat images. *Catena* **223**, 106961 (2023).
42. Yan, F., Wang, X. & Su, F. Ecosystem service changes in response to mainland coastline movements in China: process, pattern, and trade-off. *Ecol. Indic.* **116**, 106337 (2020).
43. Tian, Z., Zhang, Y., Udo, K. & Lu, X. Regional economic losses of China's coastline due to typhoon-induced port disruptions. *Ocean Coast. Manage.* **237**, 106533 (2023).
44. Wang, Y. et al. Does continuous straw returning keep China farmland soil organic carbon continued increase? A meta-analysis. *J. Environ. Manage.* **288**, 112391 (2021).
45. Zhou, Y., Ning, L. & Bai, X. Spatial and temporal changes of human disturbances and their effects on landscape patterns in the Jiangsu coastal zone, China. *Ecol. Indic.* **93**, 111–122 (2018).
46. Ju, H. et al. Spatiotemporal patterns and modifiable areal unit problems of the landscape ecological risk in coastal areas: a case study of the Shandong Peninsula, China. *J. Clean. Prod.* **310**, 127522 (2021).
47. Yang, Y., Li, H. & Qian, C. Analysis of the implementation effects of ecological restoration projects based on carbon storage and eco-environmental quality: a case study of the Yellow River Delta, China. *J. Environ. Manage.* **340**, 117929 (2023).
48. Han, B. et al. An integrated evaluation framework for Land-Space ecological restoration planning strategy making in rapidly developing area. *Ecol. Indic.* **124**, 107374 (2021).
49. Liu, F. et al. Mapping high resolution National Soil Information Grids of China. *Sci. Bull.* **67**, 328–340 (2022).
50. Lin, L. I. K. A concordance correlation coefficient to evaluate reproducibility. *Biometrics* **45**, 255 (1989).
51. Lamichhane, S., Kumar, L. & Wilson, B. Digital soil mapping algorithms and covariates for soil organic carbon mapping and their implications: a review. *Geoderma* **352**, 395–413 (2019).
52. Wang, S., Adhikari, K., Wang, Q., Jin, X. & Li, H. Role of environmental variables in the spatial distribution of soil carbon (C), nitrogen (N), and C: N ratio from the northeastern coastal agroecosystems in China. *Ecol. Indic.* **84**, 263–272 (2018).
53. Morgan, C. L. S., Waiser, T. H., Brown, D. J. & Hallmark, C. T. Simulated in situ characterization of soil organic and inorganic carbon with visible near-infrared diffuse reflectance spectroscopy. *Geoderma* **151**, 249–256 (2009).
54. Akpa, S. I. C., Odeh, I. O. A., Bishop, T. F. A., Hartemink, A. E. & Amapu, I. Y. Total soil organic carbon and carbon sequestration potential in Nigeria. *Geoderma* **271**, 202–215 (2016).
55. Liang, Z., Chen, S., Yang, Y., Zhou, Y. & Shi, Z. High-resolution three-dimensional mapping of soil organic carbon in China: effects of soilgrids products on national modeling. *Sci. Total Environ.* **685**, 480–489 (2019).
56. Yamashita, N. et al. National-scale 3D mapping of soil organic carbon in a Japanese forest considering microtopography and tephra deposition. *Geoderma* **406**, 115534 (2022).
57. Sothe, C., Gonsamo, A., Arabian, J. & Snider, J. Large scale mapping of soil organic carbon concentration with 3D machine learning and satellite observations. *Geoderma* **405**, 115402 (2022).
58. Sahu, B., Ghosh, A. K. & Seema. Deterministic and geostatistical models for predicting soil organic carbon in a 60ha farm on Inceptisol in Varanasi, India. *Geoderma Reg.* **26**, e00413 (2021).
59. Encina-Rojas, A. et al. First soil organic carbon report of Paraguay. *Geoderma Reg.* **32**, e00611 (2023).
60. Wang, H. et al. Soil organic carbon of degraded wetlands treated with freshwater in the Yellow River Delta, China. *J. Environ. Manage.* **92**, 2628–2633 (2011).
61. Liu, L., Xu, W., Yue, Q., Teng, X. & Hu, H. Problems and countermeasures of coastline protection and utilization in China. *Ocean Coast. Manage.* **153**, 124–130 (2018).
62. Tătui, F. et al. The Black Sea coastline erosion: Index-based sensitivity assessment and management-related issues. *Ocean Coast. Manage.* **182**, 104949 (2019).
63. Feng, J., Li, D., Li, D., Zhang, J. & Zhao, L. Comparison between the skew surge and residual water level along the coastline of China. *J. Hydrol.* **598**, 126299 (2021).
64. Moujabber, M. E., Samra, B. B., Darwish, T. & Atallah, T. Comparison of different indicators for groundwater contamination by seawater intrusion on the Lebanese coast. *Water Resour. Manage.* **20**, 161–180 (2006).
65. Fan, X. et al. Soil salinity development in the Yellow River Delta in relation to groundwater dynamics. *Land Degrad. Develop.* **23**, 175–189 (2012).
66. Borges, P. A. V. et al. Global Island Monitoring Scheme (GIMS): a proposal for the long-term coordinated survey and monitoring of native island forest biota. *Biodivers. Conserv.* **27**, 2567–2586 (2018).
67. Spadoni, G. L., Cavalli, A., Congedo, L. & Munafò, M. Analysis of Normalized Difference Vegetation Index (NDVI) multi-temporal series for the production of forest cartography. *Remote Sens. Appl.: Soc. Environ.* **20**, 100419 (2020).
68. Ren, H., Zhou, G. & Zhang, F. Using negative soil adjustment factor in soil-adjusted vegetation index (SAVI) for aboveground living biomass estimation in arid grasslands. *Remote Sens. Environ.* **209**, 439–445 (2018).
69. Liu, J. et al. Modeling watershed carbon dynamics as affected by land cover change and soil erosion. *Ecol. Model.* **459**, 109724 (2021).
70. Chang, X., Xing, Y., Wang, J., Yang, H. & Gong, W. Effects of land use and cover change (LUCC) on terrestrial carbon stocks in China between 2000 and 2018. *Resour. Conserv. Recy.* **182**, 106333 (2022).
71. Zhang, Z. et al. Spatiotemporal pattern of landscape ecological sensitivity in coastal zone in the last 30 years: an empirical study of Shandong Peninsula, China. *J. Coast. Conserv.* **26**, 55 (2022).
72. Xiao, L. & Zhao, R. China's new era of ecological civilization. *Science* **358**, 1008–1009 (2017).
73. Liu, Y., Fang, F. & Li, Y. Key issues of land use in China and implications for policy making. *Land Use Policy* **40**, 6–12 (2014).
74. Do, A. N. T., Tran, H. D., Ashley, M. & Nguyen, A. T. Monitoring landscape fragmentation and aboveground biomass estimation in Can Gio Mangrove Biosphere Reserve over the past 20 years. *Ecol. Inform.* **70**, 101743 (2022).
75. Li, Y., Sun, Y. & Li, J. Heterogeneous effects of climate change and human activities on annual landscape change in coastal cities of mainland China. *Ecol. Indic.* **125**, 107561 (2021).
76. Wu, Z. et al. Estimating soil organic carbon density in plains using landscape metric-based regression Kriging model. *Soil Till. Res.* **195**, 104381 (2019).
77. Abd-Elmabod, S. K., Fitch, A. C., Zhang, Z., Ali, R. R. & Jones, L. Rapid urbanisation threatens fertile agricultural land and soil carbon in the Nile delta. *J. Environ. Manage.* **252**, 109668 (2019).
78. Luo, Y. et al. Loss of organic carbon in suburban soil upon urbanization of Chengdu megacity, China. *Sci. Total Environ.* **785**, 147209 (2021).
79. Gao, M., Hu, Y. & Bai, Y. Construction of ecological security pattern in national land space from the perspective of the community of life in mountain, water, forest, field, lake and grass: a case study in Guangxi Hechi, China. *Ecol. Indic.* **139**, 108867 (2022).
80. Hao, Z., Huang, J., Li, X., Sun, H. & Fang, G. A multi-point aggregation trend of the outbreak of pine wilt disease in China over the past 20 years. *Forest Ecol. Manage.* **505**, 119890 (2022).
81. Lu, F. et al. Soil carbon sequestrations by nitrogen fertilizer application, straw return and no-tillage in China's cropland. *Glob. Chang. Biol.* **15**, 281–305 (2010).
82. Feng, Y. et al. Dynamics in soil quality and crop physiology under poplar-agriculture tillage models in coastal areas of Jiangsu, China. *Soil Till. Res.* **204**, 104733 (2020).
83. Wang, M., Wang, X., Zhou, R. & Zhang, Z. An indicator framework to evaluate the Blue Bay Remediation Project in China. *Reg. Stud. Mar. Sci.* **38**, 101349 (2020).
84. Liu, Y. & Zhou, Y. Territory spatial planning and national governance system in China. *Land Use Policy* **102**, 105288 (2021).
85. De Groot, J. J., Brus, D. J., Bierkens, M. F. P. & Knotter, M. Sampling for Natural Resource Monitoring. *Springer*, Berlin (332 pp.) (2006).
86. Chen, J., Ban, Y. & Li, S. Open access to Earth land-cover map. *Nature* **514**, 434 (2014).
87. Douaoui, A. E. K., Nicolas, H. & Walter, C. Detecting salinity hazards within a semiarid context by means of combining soil and remote-sensing data. *Geoderma* **134**, 217–230 (2006).
88. Huete, A. R. A soil-adjusted vegetation index (SAVI). *Remote Sens. Environ.* **25**, 295–309 (1988).
89. Chi, Y. et al. Evaluating landscape ecological sensitivity of an estuarine island based on landscape pattern across temporal and spatial scales. *Ecol. Indic.* **101**, 221–237 (2019).
90. Viscarra Rossel, R. A. & Behrens, T. Using data mining to model and interpret soil diffuse reflectance spectra. *Geoderma* **158**, 46–54 (2010).
91. Zhang, W., Wan, H., Zhou, M., Wu, W. & Liu, H. Soil total and organic carbon mapping and uncertainty analysis using machine learning techniques. *Ecol. Indic.* **143**, 109420 (2022).
92. Foody, G. M. Relating the land-cover composition of mixed pixels to artificial neural network classification output. *Photogramm. Eng. Rem. S.* **62**, 491–500 (1996).
93. Dai, X., Guo, Z., Zhang, L. & Wu, J. Spatio-temporal pattern of urban land cover evolution with urban renewal and expansion in Shanghai based on mixed-pixel classification for remote sensing imagery. *Int. J. Remote Sens.* **31**, 6095–6114 (2010).

Acknowledgements

This research was funded by the National Natural Science Foundation of China (No. 42071116) and the Basic Scientific Fund for National Public Research Institutes of China (No. 2021S02). We also thank the National Earth System Science Data Center, National Science & Technology Infrastructure of China (<http://www.geodata.cn>), USGS (<https://glavis.usgs.gov/>), and GlobeLand30 (www.globallandcover.com) for the open source data.

Author contributions

Y.C., D.L., and J.G. conceived the research. Y.C. designed the methodology, ran the simulations, and analyzed the results. Y.C., J.S., Z.Z., W.X., Y.Q., X.M., and B.Z. performed data acquisition. Y.C. wrote the manuscript.

Competing interests

The authors declare no competing interests.

Additional information

Supplementary information The online version contains supplementary material available at <https://doi.org/10.1038/s43247-023-01044-5>.

Correspondence and requests for materials should be addressed to Yuan Chi, Dahai Liu or Jianhua Gao.

Peer review information *Communications Earth & Environment* thanks Zhen-Ming Ge and the other, anonymous, reviewer(s) for their contribution to the peer review of this work. Primary Handling Editors: Huai Chen, Clare Davis. A peer review file is available.

Reprints and permission information is available at <http://www.nature.com/reprints>

Publisher's note Springer Nature remains neutral with regard to jurisdictional claims in published maps and institutional affiliations.



Open Access This article is licensed under a Creative Commons Attribution 4.0 International License, which permits use, sharing, adaptation, distribution and reproduction in any medium or format, as long as you give appropriate credit to the original author(s) and the source, provide a link to the Creative Commons licence, and indicate if changes were made. The images or other third party material in this article are included in the article's Creative Commons licence, unless indicated otherwise in a credit line to the material. If material is not included in the article's Creative Commons licence and your intended use is not permitted by statutory regulation or exceeds the permitted use, you will need to obtain permission directly from the copyright holder. To view a copy of this licence, visit <http://creativecommons.org/licenses/by/4.0/>.

© The Author(s) 2023